ISSN 1674-1056
http://cpb.iphy.ac.cn
http://iopscience.iop.org/cpb
中国物理 B
Chinese Physics
中国物理 Chinese Physics B

Configuration interaction calculations on the spectroscopic and transition properties of magnesium chloride

Dong-lan Wu(伍冬兰), Cheng-quan Lin(林成泉), Yu-feng Wen(温玉锋), An-dong Xie(谢安东), Bing Yan(闫冰)

Citation: Chin. Phys. B . 2018, 27(8): 083101. **doi:** 10.1088/1674-1056/27/8/083101

Journal homepage: http://cpb.iphy.ac.cn; http://iopscience.iop.org/cpb

What follows is a list of articles you may be interested in

Theoretical study of spin-forbidden cooling transitions of indium hydride using *ab initio* methods

Yun-Guang Zhang(张云光), Hua Zhang(张华), Ge Dou(窦戈)
Chin. Phys. B . 2017, 26(9): 093101. **doi:** 10.1088/1674-1056/26/9/093101

First-principles study of solute diffusion in Ni_3Al

Shaohua Liu(刘少华), Zi Li(李孜), Chongyu Wang(王崇愚)
Chin. Phys. B . 2017, 26(9): 093102. **doi:** 10.1088/1674-1056/26/9/093102

MRCI+Q study of the low-lying electronic states of CdF including spin—orbit coupling

Shu-Tao Zhao(赵书涛), Bing Yan(闫冰), Rui Li(李瑞), Shan Wu(武山), Qiu-Ling Wang(王秋玲)
Chin. Phys. B . 2017, 26(2): 023105. **doi:** 10.1088/1674-1056/26/2/023105

Multireference calculations on low-lying states and $X^3\Pi_u$-$^3\Pi_g$ absorption spectra of indium dimer

Zhou Ling-Song, Yan Bing, Jin Ming-Xing
Chin. Phys. B . 2013, 22(4): 043102. **doi:** 10.1088/1674-1056/22/4/043102

Theoretical study of potential energy curves, spectroscopic constants, and radiative lifetimes of low-lying states in SeO molecule

Li Rui, Lian Ke-Yan, Li Qi-Nan, Miao Feng-Juan, Yan Bing, Jin Ming-Xing
Chin. Phys. B . 2012, 21(12): 123102. **doi:** 10.1088/1674-1056/21/12/123102

Configuration interaction calculations on the spectroscopic and transition properties of magnesium chloride*

Dong-lan Wu(伍冬兰)[1,2], Cheng-quan Lin(林成泉)[1], Yu-feng Wen(温玉锋)[1], An-dong Xie(谢安东)[1], and Bing Yan(闫冰)[2,†]

[1] College of Mathematical and Physical Sciences, Jinggangshan University, Ji'an 343009, China
[2] Jilin Provincial Key Laboratory of Applied Atomic and Molecular Spectroscopy, Institute of Atomic and Molecular Physics, Jilin University, Changchun 130012, China

(Received 9 April 2018; revised manuscript received 24 May 2018; published online 25 July 2015)

The potential energy curves (PECs) of 14 Λ–S states for magnesium chloride (MgCl) have been calculated by using multi-reference configuration interaction method with Davidson correction (MRCI + Q). The core-valence correlation (CV), scalar relativistic effect, and spin–orbit coupling (SOC) effect are considered in the electronic structure computations. The spectroscopic constants of $X^2\Sigma^+$ and $A^2\Pi$ states have been obtained, which are in good agreement with the existing theoretical and experimental results. Furthermore, other higher electronic states are also characterized. The permanent dipole moments (PDMs) of Λ–S states and the spinorbit (SO) matrix elements between Λ–S states are also computed. The results indicate that the abrupt changes of PDMs and the SO matrix elements are attributed to the avoided crossing between the states with the same symmetry. The SOC effect is taken into account with Breit–Pauli operator, which makes the 14 Λ–S states split into 30 Ω states, and leads to a double-well potential of the $\Omega = (3)1/2$ state. The energy splitting for the $A^2\Pi$ is calculated to be 53.61 cm^{-1} and in good agreement with the experimental result 54.47 cm^{-1}. The transition dipole moments (TDMs), Franck–Condon factors (FCFs), and the corresponding radiative lifetimes of the selected transitions from excited Ω states to the ground state $X^2\Sigma + 1/2$ have been reported. The computed radiative lifetimes $\tau_{v'}$ of low-lying excites Ω states are all on the order of 10 ns. Finally, the feasibility of laser cooling of MgCl molecule has been analyzed.

Keywords: MgCl, MRCI + Q, spectroscopic and transition properties, spin–orbit coupling

PACS: 31.15.A–, 31.15.vn, 33.15.Mt **DOI:** 10.1088/1674-1056/27/8/083101

1. Introduction

The spectroscopic investigations of alkaline-earth monohalides (MgX, X = F, Cl, Br, I) have attracted much theoretical and experimental research interest for a long time.[1–6] Since the alkaline-earth monohalides are ionic molecules, these compounds can be treated with ionic bonding models,in which the Mg^+ and X^- are described as two closed-shell ion cores surrounding by an unpaired electron. The previous spectroscopic studies of ionic bonding models of MgX mainly focused on the low-lying electronic states, i.e., ground state $X^2\Sigma^+$, the first excited state $A^2\Pi$, and $B^2\Sigma^+$ state.[7–9] Very recently, the MgX were theoretically regarded as candidates for laser cooling molecules.[10,11] The accurate spectroscopic and transition properties for MgX are very helpful for designing the cooling scheme.

The previous experimental spectroscopic studies of the MgCl molecule mainly focused on two band systems $A^2\Pi$–$X^2\Sigma^+$ and $B^2\Sigma^+$–$A^2\Pi$. The vibrationally resolved absorption bands were detected by Morgan,[5] which was ascribed to $^2\Pi$–$X^2\Sigma^+$ transition. The rotational structure of $B^2\Sigma^+$–$A^2\Pi$ spectral band was discussed by Singh *et al.*,[12] and the rotational constants of $B^2\Sigma^+$ and $A^2\Pi$ were evaluated. Recently, the emission spectrum of the MgCl $A^2\Pi$–$X^2\Sigma^+$ band system was studied with high-resolution Fourier transform spectroscopy by Hiroa *et al.*,[13] and accurate spectroscopic constants of low-lying states were determined. Ohshima *et al.*[14] used a Fourier-transform microwave spectrometer to detect the rotational spectrum of $X^2\Sigma^+$ ($v = 0, 1$), and obtained hyperfine coupling constants. The $B^2\Sigma^+$–$A^2\Pi$ band system in the 4500 Å–5000 Å region was observed by Rao and Rao,[15] and $A^2\Pi$ was assigned by the vibrational analysis of the spectral band system. Darji *et al.*[16] confirmed the vibrational analysis given by Rao and Rao[15] using the isotope-shifts studies. Later, Singh *et al.* observed the $B^2\Sigma^+$–$A^2\Pi$ (0,0) band,[17] from which the perturbations from $^2\Pi_i$ state to the $v = 0$ of $B^2\Sigma^+$ state were discussed.

In the aspect of theoretical investigations, Parlant *et al.*[18] carried out *ab initio* calculations by using first and secondorder configuration interaction (SOCI) on MgCl. They investigated the predissociation mechanisms of $A^2\Pi$ state via the interstate coupling and spin–orbit coupling (SOC) interaction. Bogey *et al.*[19] analyzed the rotational spectrum of the ground state and obtained the rotationally resolved molecular constants. Parlant *et al.*[18] analyzed the SOC splits of $A^2\Pi$ state. Our previ-

*Project supported by the National Natural Science Foundation of China (Grand Nos. 11564019, 11147158, 11264020, and 11574114) and Jiangxi Provincial Education Department Project, China (Grand No. GJJ170654).

†Corresponding author. E-mail: yanbing@jlu.edu.cn

© 2018 Chinese Physical Society and IOP Publishing Ltd

ous report[20] investigated radiative transition probabilities of $A^2\Pi$–$X^2\Sigma^+$ transition by employing the MRCI + Q method. Recently, Wan *et al.*[4] utilized MRCI method to calculate the potential energy curves of $X^2\Sigma^+$, $A^2\Pi$, and $2^2\Pi$ of MgCl, and the laser cooling mechanism based on $A^2\Pi$–$X^2\Sigma^+$ transition was discussed. As mentioned above, the spectroscopic and transition properties of low-lying electronic states in MgCl were previously reported, while in these computational studies, the core-valence correlation and scalar relativistic effect were not fully considered. To the best of our knowledge, the studies of spectroscopic parameters and transition properties of MgCl have been focused on the ground state $X^2\Sigma^+$ and excited states $A^2\Pi$, $B^2\Sigma^+$, and $C^2\Pi$.[10,13,17] However, other higher excited states of MgCl have not been studied in previous work, and it may provide extensive and accurate information for the electronic structure of MgCl system.

In this work, we perform high-level *ab initio* calculations on the MgCl molecule. The potential energy curves (PECs) of the 14Λ–S states for the MgCl molecule, as well as those of 30 Ω states generated from the Λ–S states are computed with multireference configuration interaction method including Davidson correction (MRCI + Q). Based on the computed Λ–S compositions of the Ω states, the configurations mixings of some Λ–S states are analyzed. The transition properties are also predicted including transition dipole moments (TDMs), Franck–Condon factors, and the radiative lifetimes.

2. Computational method

All the *ab initio* calculations of MgCl are carried out by employing the MOLPRO 2012 quantum chemistry package.[21,22] The C_{2v} point group is used for MgCl in the calculations, which includes $A_1/B_1/B_2/A_2$ irreducible representations. For MgCl, $4a_1$, $2b_1$, and $2b_2$ symmetry molecular orbitals corresponding to the 3s3p shells for Mg and Cl are selected as the active space, Hence, the $3s^2$ electrons for Mg and $3s^23p^5$ electrons for Cl are put into the active space. All $2s^22p^6$ electrons in the inner shell of Mg are put into the closed-shell, and these orbitals are doubly occupied in all reference configuration state functions, but correlated through singly and doubly excitations in MRCI computations. The remaining inner electrons are put into the core orbitals. That is to say, there are a total of 17 electrons in the correlation energy calculations.

In order to obtain accurate PECs of MgCl, the potential energies at a set of bond lengths are calculated using the state-averaged complete active space self-consistent field (SA-CASSCF)[23,24] approach followed by the internally contracted multireference configuration interaction method including the Davidson correction (icMRCI + Q).[25–28] The third-order Douglas–Kroll integrals have been utilized to calculate the scalar relativity effect.[29] As for the basis set, the correlation-consistent aug-cc-pwCV5Z-DK basis set[30] and aug-cc-pV5Z-DK basis set[31] are employed for Mg and Cl, respectively. The PECs of these 14 Λ–S electronic states are drawn with the help of the avoided crossing rule of the same symmetry.

Moreover, the SOC effect is treated by the state interaction method with the full Breit–Pauli Hamiltonian[32] via a two-step perturbative procedure. The off-diagonal SO matrix elements are determined from the MRCI wavefunctions, while the diagonal SO matrix elements are substituted by the ic-MRCI + Q energies. The SOC effect makes the 14 Λ–S states split into 30 Ω states. The PECs of Ω states are constructed by our calculated energies with the aid of the avoided crossing rule.

Based on the calculated PECs of the Λ–S and Ω states, the spectroscopic constants are determined by solving the radial Schrödinger equations of nuclear motion using the LEVEL8.0 program,[33] which include equilibrium internuclear distance R_e, excitation energy T_e, vibrational constants ω_e and $\omega_e\chi_e$, balanced rotation constant B_e, and vibration-rotation coupling constant α_e. The dissociation energy D_e is obtained by subtracting the molecular energy at R_e from the energy at a large separation. The SO matrix elements between electronic states were computed and used to analyze the coupling between the interacting Λ–S states. The TDMs are calculated at the MRCI level. The Franck–Condon factors (FCFs) are evaluated with the LEVEL8.0 program.[33] And the radiative lifetimes of the several lowest transitions are predicted based on the calculated TDMs and Franck–Condon (FC) factors.

3. Results and discussion

3.1. The PECs of the 14 Λ–S states

All 14 Λ–S states of MgCl molecule have been studied by using the ic-MRCI + Q method with aug-cc-pwCV5Z-DK for Mg and aug-cc-pV5Z-DK for Cl, respectively. The single-point energies at a series of internuclear distances from 1.5 Å to 5 Å are calculated. The corresponding PECs are depicted in Fig. 1. The overall shape of PECs for MgCl is similar to that of its isovalent system MgBr investigated in our previous work.[34] As shown in Fig. 1, the 14 Λ–S states are associated with three dissociation limits, i.e., neutral Mg $(^1S_g) + Cl\ (^2P_u)$, Mg $(^3P_u) + Cl\ (^2P_u)$, and ion-pair $Mg^+(^2S_g) + Cl^-(^1S_g)$. And only the $B^2\Sigma^+$ state is associated with the ion-pair limit $Mg^+(^2S_g) + Cl^-(^1S_g)$, which corresponds to the one-electron transfer from Mg to Cl. The spectroscopic constants of doublet states $X^2\Sigma^+$, $A^2\Pi$, $B^2\Sigma^+$, $C^2\Pi$, and $3^2\Sigma^+$ are fitted by the calculated PECs and listed in Table 1, along with their main electronic configurations and weights around R_e. For comparison, the available experimental and other theoretical results are also listed in Table 1.

Table 1. The spectroscopic constants of the bound Λ–S states of MgCl molecule.

Λ−S state	T_e/cm^{-1}	R_e/Å	ω_e/cm^{-1}	$\omega_e\chi_e$/cm^{-1}	B_e/cm^{-1}	$10^2\alpha_e$/cm^{-1}	D_e/eV	Main configuration at R_e/%
$X^2\Sigma^+$	0.0	2.2140	460.44	1.8873	0.2418	0.1533	3.325	$7\sigma^2 8\sigma^2 9\sigma^\alpha 10\sigma^0 3\pi^4 4\pi^0$ (84.6)
								$7\sigma^2 8\sigma^2 9\sigma^0 10\sigma^\alpha 3\pi^4 4\pi^0$ (4.0)
Calc.[a]	0.0	2.2025	467.53	–	0.2409	–	3.302	
Expt.[b]	0.0	–	462.10	1.381	0.2456	0.162	2.726	
Expt.[c]	0.0	2.196	466.08	2.0	0.2456	0.161	3.37	
Expt.[d]	0.0	2.1991	462.12	2.10	0.2450	0.1580	–	
$A^2\Pi$	26580	2.1855	506.02	2.6716	0.2481	0.1299	0.552	$7\sigma^2 8\sigma^2 9\sigma^0 10\sigma^0 3\pi^4 4\pi^\alpha$ (85.1)
								$7\sigma^2 8\sigma^\alpha 9\sigma^\beta 10\sigma^0 3\pi^4 4\pi^\alpha$ (1.8)
								$7\sigma^2 8\sigma^2 9\sigma^2 10\sigma^0 3\pi^{\alpha\alpha\beta} 4\pi^0$ (1.0)
Calc.[a]	26062.04	2.1777	492.33	–	0.2465	–	0.5359	
Expt.[c]	26496.4	2.169	490.8	2.18	0.2517	0.165	3.42	
Expt.[b]	26739.91	–	-	2.6693	0.2508	–	-	
$B^2\Sigma^+$(int)	38274	2.1660	472.71	14.0226	0.2551	0.182	0.124	$7\sigma^2 8\sigma^\alpha 9\sigma^2 10\sigma^0 3\pi^4 4\pi^0$ (41.7)
								$7\sigma^2 8\sigma^2 9\sigma^\alpha 10\sigma^0 3\pi^4 4\pi^0$ (34.3)
								$7\sigma^2 8\sigma^\alpha 9\sigma^\beta 10\sigma^\alpha 3\pi^4 4\pi^0$ (4.1)
								$7\sigma^2 8\sigma^2 9\sigma^0 10\sigma^\alpha 3\pi^4 4\pi^0$ (3.1)
								$7\sigma^2 8\sigma^\alpha 9\sigma^\alpha 10\sigma^\beta 3\pi^4 4\pi^0$ (2.9)
$B^2\Sigma^+$(ext)	29453	3.8595	171.77	0.8381	0.0796	−0.0602	–	
$C^2\Pi$	31894	2.5605	705.16	16.8514	0.1803	0.0408	1.982	$7\sigma^2 8\sigma^2 9\sigma^0 10\sigma^0 3\pi^4 4\pi^\alpha$ (47.7)
								$7\sigma^2 8\sigma^2 9\sigma^2 10\sigma^0 3\pi^{\alpha\alpha\beta} 4\pi^0$ (35.3)
								$7\sigma^2 8\sigma^\alpha 9\sigma^\beta 10\sigma^0 3\pi^4 4\pi^\alpha$ (3.4)
								$7\sigma^2 8\sigma^2 9\sigma^0 10\sigma^0 3\pi^{\alpha\alpha\beta} 4\pi^2$ (1.2)
Calc.[a]	31946	2.5541	622.72	–	0.1793	–	2.0132	
$3^2\Sigma^+$	41770	2.4150	693.34	18.1108	0.2032	0.164	0.753	$7\sigma^2 8\sigma^2 9\sigma^0 10\sigma^\alpha 3\pi^4 4\pi^0$ (43.9)
								$7\sigma^2 8\sigma^\alpha 9\sigma^2 10\sigma^0 3\pi^4 4\pi^0$ (23.7)
								$7\sigma^2 8\sigma^2 9\sigma^\alpha 10\sigma^0 3\pi^{\alpha\beta\beta} 4\pi^\alpha$ (13.0)
								$7\sigma^2 8\sigma^2 9\sigma^\alpha 10\sigma^0 3\pi^{\alpha\beta\beta} 4\pi^\beta$ (2.5)
								$7\sigma^2 8\sigma^2 9\sigma^\alpha 10\sigma^0 3\pi^4 4\pi^0$ (1.9)
								$7\sigma^2 8\sigma^\alpha 9\sigma^\beta 10\sigma^\alpha 3\pi^4 4\pi^0$ (1.1)

[a]Ref. [10], [b]Ref. [13], [c]Ref. [36], [d]Ref. [35]

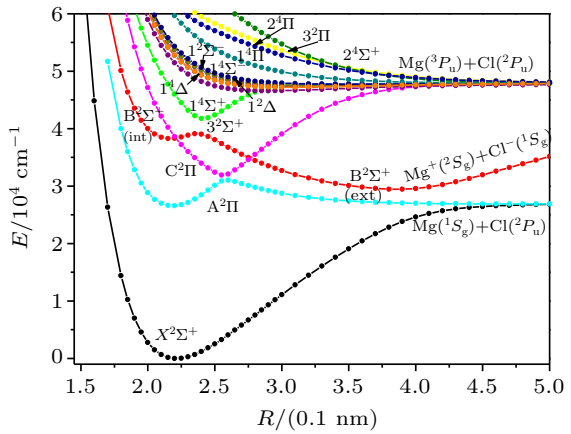


Fig. 1. (color online) The PECs of the Λ–S states of MgCl molecule.

As shown in Fig. 1, the ground state $X^2\Sigma^+$ is separated from the other electronic states and correlated with the lowest dissociation limit Mg (^1S_g) + Cl (^2P_u). The state is mainly characterized by the closed-shell electronic configuration $7\sigma^2 8\sigma^2 9\sigma^\alpha 10\sigma^0 3\pi^4 4\pi^0$, which corresponds to one-electron movement from 3s orbital of Mg to 3p orbital of Cl. For the $X^2\Sigma^+$ state, our calculated values of ω_e, $\omega_e\chi_e$, B_e, R_e, and α_e well reproduce the experimental data[35] with deviations of 1.685 cm^{-1} (0.36%), 0.1127 cm^{-1} (5.37%), 0.0032 cm^{-1} (1.31%), 0.0149 Å (0.68%), and 0.47 cm^{-1} (2.97%), respectively. This agreement is better than the recent computed results by Wan.[10] Our calculations indicate that the ground state has a deep potential well 3.325 eV, which is close to the experimental value 3.37 eV.[36]

The first excited state $A^2\Pi$ also correlates with Mg (^1S_g) + Cl (^2P_u). In Franck–Condon region, the $A^2\Pi$ state is mainly described by the electronic configuration $7\sigma^2 8\sigma^2 9\sigma^0 10\sigma^0 3\pi^4 4\pi^\alpha$, which corresponds to one-electron excitation from $X^2\Sigma^+$ state, namely, $9\sigma \rightarrow 4\pi$. The calculated T_e of 26580 cm^{-1} differs from the experimental value of 26739.91 cm^{-1} by 159.91 cm^{-1} (0.5%).[13] There is an obvious barrier owing to an avoided crossing near 2.55 Å, which locates 31030 cm^{-1} above the ground state. The calculated dissociation energy D_e is 0.552 eV, which is much smaller than that of the ground state. Our computed $\omega_e\chi_e$ result differs from the experiment[13] by 0.002 cm^{-1}. The other spectroscopic constants B_e, R_e, D_e, and ω_e are generally consistent with the recent theoretical results,[10] with percent errors of 0.65%, 0.36%, 3.0%, and 2.78%, respectively. The $C^2\Pi$ state correlates to the second neutral dissociation limit Mg (^3P_u) + Cl (^2P_u). From Fig. 1, we find that the energy minimum of $C^2\Pi$ state and the maximum energy of $A^2\Pi$ state is located at the avoided crossing point (R_{ACP}) between the $C^2\Pi$ and $A^2\Pi$ states, and the energy gap is 925.66 cm^{-1}.

The computed D_e value of 1.982 eV is much larger than that of the A state, but accords with the recent theoretical result 2.0132 eV.[10] Furthermore, the calculated B_e, R_e, and ω_e data of $C^2\Pi$ state are in good agreement with the recent theoretical results too.[10]

Of particular note is the $B^2\Sigma^+$ state, which is the only one state correlating to the ion-pair $Mg^+(^2S_g) + Cl^-(^1S_g)$. The PECs of $B^2\Sigma^+$ state is characterized by a double-well structure, with the equilibrium internuclear distance of 2.1660 Å and 3.860 Å, and the calculated T_e of 38274 cm^{-1} and 29453 cm^{-1}, respectively. The wavefunction of the $B^2\Sigma^+$ state exhibits the obvious multi-configuration character, which is made up of two main electronic configurations $7\sigma^2 8\sigma^\alpha 9\sigma^2 10\sigma^0 3\pi^4 4\pi^0$ (41.7%) and $7\sigma^2 8\sigma^2 9\sigma^\alpha 10\sigma^0 3\pi^4 4\pi^0$ (34.3%) at R_e, indicating the mixture of covalence bond and ionic bond. As for other excited electronic states, there are very few theoretical or experimental studies reported in the literatures. So, our computed spectroscopic constants with ic-MRCI+Q method will provide accurate spectroscopic information of the MgCl molecule.

Compared with other homologues, the calculated ground state D_e (3.325 eV) of MgCl is smaller than that of MgF (4.67 eV),[37] but larger than 3.157 eV of MgBr[34] for $X^2\Sigma^+$ state. The excitation energy T_e for $A^2\Pi$, $B^2\Sigma^+$, and $C^2\Pi$ excited states of MgCl is 26580 cm^{-1}, 29453 cm^{-1}, and 31894 cm^{-1}, respectively, which is a little smaller than that of MgF (27935 cm^{-1}, 38431 cm^{-1}, and 47969 cm^{-1}),[37] and larger than that of MgBr (25891 cm^{-1}, 26539 cm^{-1}, and 29096 cm^{-1}).[34] The calculated R_e values are 2.2140 Å, 2.1855 Å, 3.8595 Å, and 2.5605 Å, which are larger than those of MgF (1.7611 Å, 1.7470 Å, 3.5848 Å, and 2.3000 Å),[37] while smaller than those of MgBr (2.3710 Å, 2.3365 Å, 3.8950 Å, and 2.6275 Å).[34] The ω_e values are 460.44 cm^{-1}, 506.02 cm^{-1}, 171.77 cm^{-1}, and 705.16 cm^{-1}, which are smaller than those of MgF (555.00 cm^{-1}, 653.10 cm^{-1}, 263.60 cm^{-1}, and 1001.30 cm^{-1})[37] and larger than those of MgBr (369.21 cm^{-1}, 407.69 cm^{-1}, 146.06 cm^{-1}, and 605.46 cm^{-1}).[34] As can be seen from the above, all the spectroscopic constants show an obvious trend of change as the atomic number of the halogen atoms increases from F element to Br element.

The permanent dipole moments (PDMs) as the internuclear distance R changes from 1.5 Å to 5.0 Å are calculated and depicted in Fig. 2. It is found that the PDMs of each state change with the increase of the bond distance. Especially at large distance, the PDMs of all states exhibit two asymptotic limits due to the two different dissociation limits, namely neutral Mg + Cl and ion-pair $Mg^+ + Cl$. In detail, the calculated PDMs of all states except $B^2\Sigma^+$ state lead to consistent asymptotic limit of 0 a.u. corresponding to the dissociation limit of Mg + Cl. The PDM of $B^2\Sigma^+$ state is negative and shows linear dependence on R at large bond distance, demonstrating that the dissociation limit is $Mg^+ + Cl$ instead.

Another interesting feature to note in Fig. 2 is that a pair of complementary abrupt change of the PDMs of the $A^2\Pi$ state and $C^2\Pi$ state around the bond distance of $R_{ACP} = 2.55$ Å. Such abrupt change of the PDMs can be explained by the fact that the main electronic configuration of the $A^2\Pi$ state is $7\sigma^2 8\sigma^2 9\sigma^0 10\sigma^0 3\pi^4 4\pi^\alpha$ and the $C^2\Pi$ state becomes $(7\sigma^2 8\sigma^2 9\sigma^2 10\sigma^0 3\pi^{\alpha\alpha\beta} 4\pi^0)$ through R_{ACP}, which can be seen from Fig. 2, thus leading to the abrupt changes in the avoided crossing region.

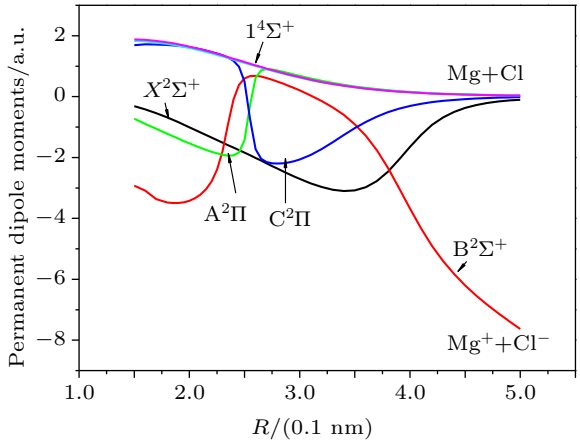


Fig. 2. (color online) The permanent dipole moments of the Λ–S states of MgCl as a function of the bond distance.

3.2. The PECs of the 30 Ω states

The SOC effect could lead to the strong interaction between the adjacent electronic states, especially the states involving the PECs' intersection. And the interaction could be quantitatively evaluated by the spin–orbit (SO) matrix element. The larger spin–orbit matrix element indicates great interaction between different electronic states. These phenomena in molecules have attracted much research interest in the previous investigations.[38–40] Figure 3 only shows the R-dependent SO matrix elements of five interaction systems including $B^2\Sigma^+$–$A^2\Pi$, $B^2\Sigma^+$–$C^2\Pi$, $3^2\Sigma^+$–$C^2\Pi$, $A^2\Pi$–$1^4\Sigma^+$, and $C^2\Pi$–$1^4\Sigma^+$ for the MgCl.

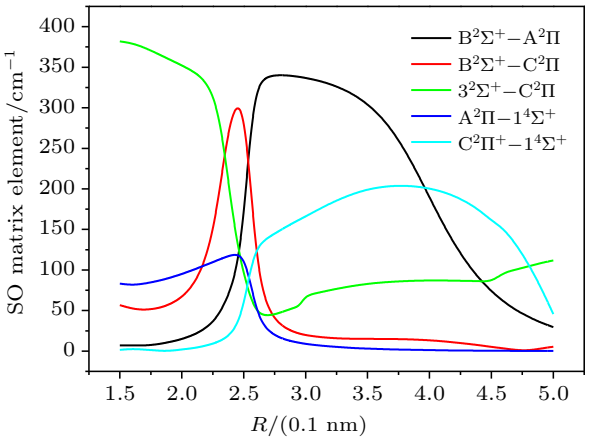


Fig. 3. (color online) The R-dependent spin–orbit matrix elements involving the $A^2\Pi$, $B^2\Sigma^+$, $C^2\Pi$, $3^2\Sigma^+$, and $1^4\Sigma^+$ states.

The SO matrix elements have the largest values 298 cm^{-1} for the $B^2\Sigma^+$–$C^2\Pi$ system after the avoided crossing point of

the $B^2\Sigma^+$ and $3^2\Sigma^+$ states, indicating the strong interaction between the $B^2\Sigma^+$ and $C^2\Pi$ state. The system $B^2\Sigma^+$–$A^2\Pi$ have larger SO matrix elements 340 cm^{-1}, which also shows the strong interaction between the $B^2\Sigma^+$ and $A^2\Pi$ states. Therefore, the perturbation of $B^2\Sigma^+$ state is mainly arising from the $A^2\Pi$ and $C^2\Pi$ states, which is consistent with the analysis in the literature.[17] The matrix element is only about 79 cm^{-1} for the crossing point of the $B^2\Sigma^+$ and $1^4\Sigma^+$ states, indicating weak interaction induced between the $B^2\Sigma^+$ and $1^4\Sigma^+$ states. As discussed above, four pairs of the complementary sudden changes have been exhibited, all of which result from the PECs' avoided crossings of $B^2\Sigma^+$ and $3^2\Sigma^+$ states, $A^2\Pi$ and $C^2\Pi$ states, and the crossing of $B^2\Sigma^+$ and $C^2\Pi$ states.

When the SOC effects are taken into account, 30 Ω states, including fifteen $\Omega = 1/2$ states, ten $\Omega = 3/2$ states, four $\Omega = 5/2$ states, and one $\Omega = 7/2$ state, are generated from the 14 Λ–S states of MgCl. Eight dissociation limits Mg $(^1S_{0g}) + Cl\ (^2P_{3/2u})$, Mg $(^1S_{0g}) + Cl\ (^2P_{1/2u})$, Mg $(^3P_{0u}) + Cl\ (^2P_{3/2u})$, Mg $(^3P_{1u}) + Cl\ (^2P_{3/2u})$, Mg $(^3P_{2u}) + Cl\ (^2P_{3/2u})$, Mg $(^3P_{0u}) + Cl\ (^2P_{1/2u})$, Mg $(^3P_{1u}) + Cl\ (^2P_{1/2u})$, and Mg $(^3P_{2u}) + Cl\ (^2P_{1/2u})$ are generated from the original Λ–S atomic limits Mg $(^1S_g) + Cl\ (^2P_u)$ and Mg $(^3P_u) + Cl\ (^2P_u)$. The detailed dissociation relationships are listed in Table 2.

The calculated atomic energy intervals of Mg and Cl are 21682.361 cm^{-1} for Mg $(^1S_{0g})$–Mg $(^3P_{0u})$, 18.292 cm^{-1} for Mg $(^3P_{1u})$–Mg (^3P_u), 46.847 cm^{-1} for Mg $(^3P_{2u})$–Mg $(^3P_{1u})$, and 836.325 cm^{-1} for Cl $(^2P_{1/2u})$–Cl $(^2P_{3/2u})$, which are in good accordance with the corresponding observed values 21850.405, 20.059, 40.714, and 882.350 cm^{-1}.[41] The PECs of 30 Ω states are depicted in Fig. 4, which are correlated with 8 dissociation limits. The spectroscopic constants of the bound states obtained by fitting the PECs, and the main Λ–S compositions at R_e are listed in Table 3.

The ground state $X^2\Sigma + 1/2$ is almost completely composed of $X^2\Sigma^+\Lambda$–S state, hence, the spectroscopic constants are hardly influenced by the SOC effect. However, slight change (only 0.0028 eV) can be found for the dissociation energy D_e after considering the SOC effect, which mainly comes from the SO splitting of Cl atom. The $A^2\Pi$ state splits into two bound Ω states of 1/2 and 3/2 state. The wave functions of these two states are mainly a mixture of B and a small part of C states, and the effect of SOC is mainly reflected in T_e and D_e. We also find that the calculated SO splitting is 53.61 cm^{-1}, which is in good agreement with the experimental observation[13] 54.47 cm^{-1} and the recent theoretical result 51.24 cm^{-1}.[10] Considering the SOC effect and the avoided crossing rule, the PECs will become complicated. From Fig. 4, the $\Omega = (3)1/2$ state is characterized by double-well potential resulting from the avoided crossing with the $(4)1/2$. The inner well mainly consists of the $B^2\Sigma^+$ state and the external one from the $C^2\Pi$ state. The spectroscopic constants of $\Omega = (4)1/2$ are greatly different from those of the Λ–S states. It is mainly due to the varying wavefunction at the equilibrium position, and the wavefunction consists of the Λ–S components $B^2\Sigma^+$ (98.65%), $A^2\Pi$ (0.27%), and $C^2\Pi$ (0.4%). For the higher-energy states, because of the high state density of the Λ–S states, the SOC leads to stronger mixture of the Λ–S components and more complicated shapes of the PECs, especially for the $\Omega = 1/2$ states. In view of the above, the SOC effects should be taken into account for the spectroscopy study of excited states of MgCl.

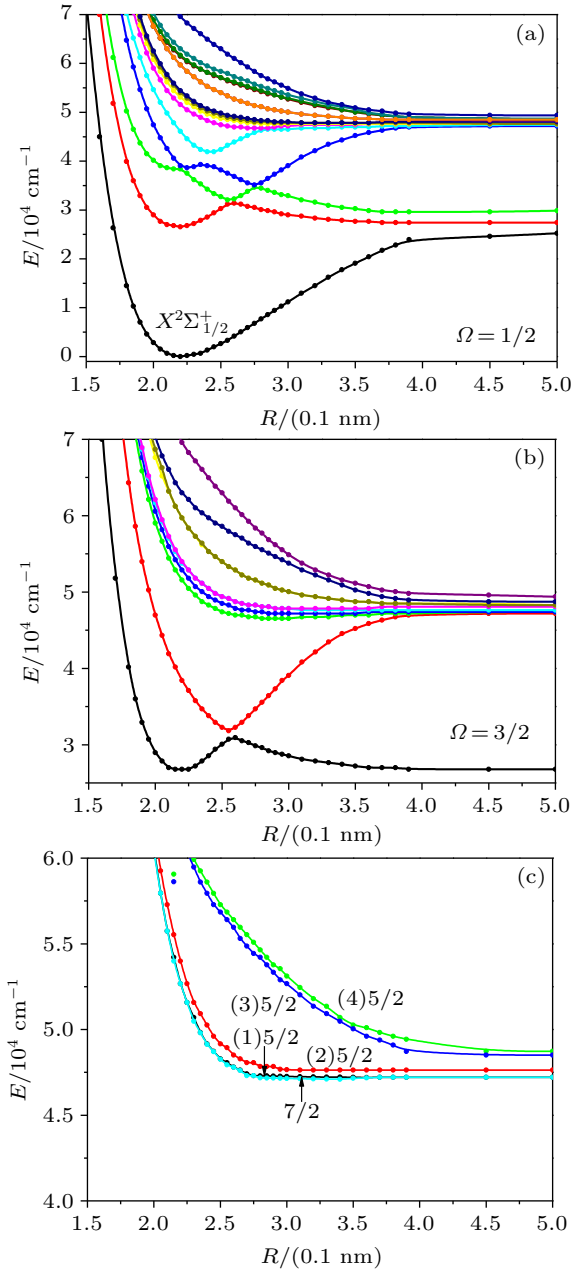


Fig. 4. (color online) The PECs of the Ω states (a) $\Omega = 1/2$, (b) $\Omega = 3/2$, (c) $\Omega = 5/2$, and $\Omega = 7/2$.

Table 2. The dissociation relationships of the Ω states of MgCl molecule.

Ω state	Atomic state	Energy/cm^{-1}	
		This work	Expt.[a]
(1) 1/2, 3/2	Mg($^1S_{0g}$)+Cl($^2P_{3/2u}$)	0	0
(2) 1/2	Mg($^1S_{0g}$)+Cl($^2P_{1/2u}$)	836.325	882.350
(3) 1/2, 3/2	Mg($^3P_{0u}$)+Cl($^2P_{3/2u}$)	21682.361	21850.405
(4) 1/2, 1/2, 3/2, 3/2, 5/2	Mg($^3P_{1u}$)+Cl($^2P_{3/2u}$)	21700.653	21870.464
(5) 1/2, 1/2, 1/2, 1/2, 3/2, 3/2, 3/2, 5/2, 5/2, 7/2	Mg($^3P_{2u}$)+Cl($^2P_{3/2u}$)	21747.500	21911.178
(6) 1/2	Mg($^3P_{0u}$)+Cl($^2P_{1/2u}$)	22518.686	22732.755
(7) 1/2, 1/2, 3/2	Mg($^3P_{1u}$)+Cl($^2P_{1/2u}$)	22526.978	22752.814
(8) 1/2, 1/2, 3/2, 3/2, 5/2	Mg($^3P_{2u}$)+Cl($^2P_{1/2u}$)	22583.825	22793.528

[a]Ref. [41]

Table 3. The spectroscopic constants of the bound Ω states of MgCl molecule.

Ω state	T_e/cm^{-1}	R_e/Å	ω_e/cm^{-1}	$\omega_e\chi_e$/cm^{-1}	B_e/cm^{-1}	$10^3\alpha_e$/cm^{-1}	D_e/cm^{-1}	Dominant Λ–S state compositions at R_e/%
$X^2\Sigma+1/2$	0	2.1990	457.7852	1.6577	0.2466	3.061	3.129	$X^2\Sigma^+$(100.00)
(2)1/2	26542.8281	2.2020	518.7415	3.4840	0.2448	−0.084	0.632	$A^2\Pi$ (100.00)
Calc.[a]	26088.05	2.1779	495.04	–	0.2465	–	0.5588	
Expt.[b]	26523	2.1720	491.6	2.54	0.25116	0.18	0.225	
(1)3/2	26489.2210	2.5890	324.2912	−21.4035	0.0692	−28.20	0.517	$A^2\Pi$ (99.44), $C^2\Pi$ (0.56)
Calc.[a]	26036.81	2.1776	492.79	–	0.2465	–	0.5112	
Expt.[b]	26469	2.1808	–	–	0.24914	0.18	0.225	
(3)1/2	29609.6814	2.1840	30.0203	−3.1967	0.0672	−1.096	–	$B^2\Sigma^+$(96.02), $C^2\Pi$ (3.98)
Calc.[a]	31974.91	2.5667	635.54	–	0.1777	–	2.0112	
(2)3/2	31823.8750	2.5500	703.8730	17.0073	0.1822	−0.176	0.665	$C^2\Pi$ (98.28), $A^2\Pi$ (1.72)
Calc.[a]	31777.98	2.5401	616.72	–	0.1880	–	2.0324	
(4)1/2	35115.6550	2.7510	726.8675	28.5025	0.1562	−2.492	1.469	$B^2\Sigma^+$(98.65), $A^2\Pi$ (0.27), $C^2\Pi$ (0.4)
(5)1/2	41867.8208	2.4240	770.9581	28.8308	0.2015	1.646	0.680	$3^2\Sigma^+$(99.91), $C^2\Pi$ (0.03)
(6)1/2	46722.1250	2.7195	229.3885	13.9397	0.1535	1.680	0.109	$1^4\Sigma^+$(97.90), $1^4\Sigma^-$(0.38)

[a]Ref. [10], [b]Ref. [13]

From the above analysis, it can be seen that the change of the wavefunction lead to the change of spectroscopic constant for Ω state. In order to illustrate the Λ–S component mixture in the wavefunction of the Ω state, we provide the R-dependent Λ–S components in the wavefunctions of the $\Omega = (2)1/2$, $(3)1/2$, $(1)3/2$, and $(2)3/2$ states. As shown in Fig. 5, the $(2)1/2$ state is mainly from SOC splitting of the $A^2\Pi$ state. Due to the obvious mixture with $C^2\Pi$, the paired peak values of the percentages suddenly appear near 2.55 Å, which is just at the avoided crossing position between the $A^2\Pi$ and $C^2\Pi$ states in Fig. 1. The adjacent $B^2\Sigma^+$ and $X^2\Sigma^+$ states contribute to the $(2)1/2$ state at $R > 4.0$ Å region, especially the $X^2\Sigma^+$ state. As for the $\Omega = (1)3/2$ state, it derives from the $\Omega = (1)3/2$ component of the $A^2\Pi$ state with a slight mixture of $C^2\Pi$ state near the avoided crossing point at 2.55 Å. The $(3)1/2$ state, as mentioned before, is characterized by the double-well potential and the Λ–S components switch between the $C^2\Pi$ and $B^2\Sigma^+$ states in the avoided crossing region. For the $(2)3/2$ state, the mixture is relatively simple at small internuclear instance, but becomes very complex at large internuclear instance.

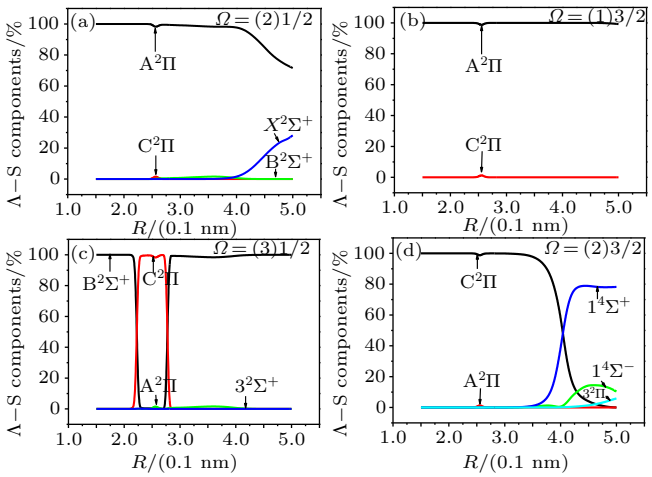


Fig. 5. (color online) The Λ–S component of 1/2 and 3/2 (a) $\Omega = (2)1/2$, (b) $\Omega = (1)3/2$, (c) $\Omega = (3)1/2$, and (d) $\Omega = (2)3/2$.

3.3. The transition properties and the radiative lifetimes

Figure 6 shows the absolute values for transition dipole moments of $(2)1/2$–$X^2\Sigma+1/2$, $(3)1/2$–$X^2\Sigma+1/2$, $(4)1/2$–$X^2\Sigma+1/2$, $(1)3/2$–$X^2\Sigma+1/2$, and $(2)3/2$–$X^2\Sigma+1/2$ as a function of the internuclear distance. As illustrated in Fig. 6, the TDMs curves exhibit four paired abrupt changes around the avoided crossing points (R_{1ACP}, R_{2ACP}, R_{3ACP}, and

R_{4ACP}), resulting from the avoided crossing with the adjacent Ω states of the same symmetry. Both of the transitions $(2)1/2$–$X^2\Sigma+1/2$ and $(1)3/2$–$X^2\Sigma+1/2$, arising from $A^2\Pi$–$X^2\Sigma^+$ transition of Λ–S states, have relative large TDMs about 2.0 a.u. at $R<2.5$ Å. It can be found that the abrupt changes of the TDMs value are observed between the $(2)1/2$–$X^2\Sigma+1/2$ and $(3)1/2$–$X^2\Sigma+1/2$ at $R_{1ACP}=2.55$ Å, which may result from the avoided crossing of $A^2\Pi$ and $C^2\Pi$ states. Due to the avoided crossing between $(3)1/2$ and $(4)1/2$ states, the $(3)1/2$–$X^2\Sigma+1/2$ transition is mainly characterized by the transition $B^2\Sigma^+$–$X^2\Sigma^+$ in the bond region from 2.36 Å (R_{3ACP}) to 2.93 Å (R_{4ACP}). Both $(1)3/2$–$X^2\Sigma+1/2$ and $(2)3/2$–$X^2\Sigma+1/2$ transitions have large TDMs. It is worth noting that the TDMs have abrupt changes near 2.50 Å (R_{2ACP}), which is due to the avoided crossing between the $A^2\Pi$ and $C^2\Pi$ states as well.

The Franck–Condon factors of all the transitions mentioned have been evaluated with the aid of the LEVEL program and listed in Table 4. From Table 4, it can be seen that the transitions $(2)1/2$–$X^2\Sigma+1/2$ and $(1)3/2$–$X^2\Sigma+1/2$ have the maximum FC factors 0.981740 and 0.976493 for 0–0 vibrational transition, which is due to the similar equilibrium

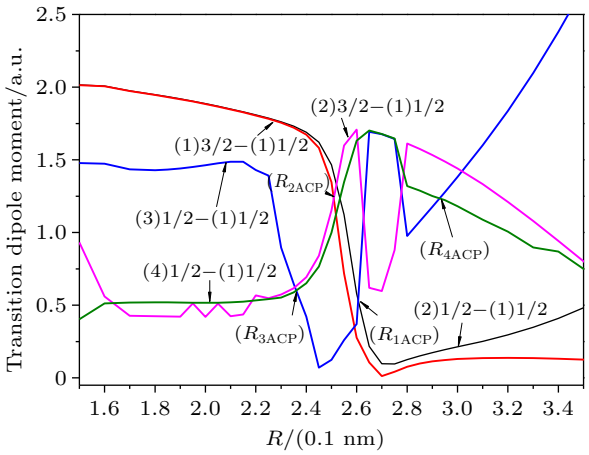


Fig. 6. (color online) The TDMs of the transitions $(2)1/2$–$X^2\Sigma+1/2$, $(3)1/2$–$X^2\Sigma+1/2$, $(4)1/2$–$X^2\Sigma+1/2$, $(1)3/2$–$X^2\Sigma+1/2$, and $(2)3/2$–$X^2\Sigma+1/2$.

Table 4. The FC factors of the transitions $(2)1/2$–$X^2\Sigma+1/2$, $(3)1/2$–$X^2\Sigma+1/2$, $(1)3/2$–$X^2\Sigma+1/2$, and $(2)3/2$–$X^2\Sigma+1/2$.

	$v''=0$	1	2	3	4	5	6	7	8	9	10	11	12	13
						$(2)1/2$–$X^2\Sigma+1/2$								
$v'=0$	0.981740	0.016767	0.000022	0.000879	0.000551	0.000005	0.000027	0.000008	0.000000	0.000000	0.000000	0.000000	0.000000	0.000000
1	0.014696	0.788990	0.187963	0.005826	0.001042	0.001221	0.000149	0.000061	0.000081	0.000000	0.000000	0.000000	0.000000	0.000000
2	0.000955	0.165430	0.544836	0.265918	0.021149	0.000582	0.000485	0.000390	0.000008	0.000000	0.000000	0.000000	0.000000	0.000000
3	0.002387	0.021354	0.234583	0.427038	0.268107	0.043827	0.002100	0.000079	0.000226	0.000000	0.000000	0.000000	0.000000	0.000000
4	0.000132	0.006772	0.028831	0.263430	0.349897	0.286252	0.058885	0.005350	0.000121	0.000000	0.000000	0.000000	0.000000	0.000000
5	0.000083	0.000085	0.003195	0.033505	0.295180	0.242571	0.330050	0.084592	0.008950	0.000000	0.000000	0.000000	0.000000	0.000000
6	0.000004	0.000506	0.000000	0.002993	0.056495	0.320664	0.132187	0.342704	0.119227	0.000000	0.000000	0.000000	0.000000	0.000000
7	0.000000	0.000008	0.000393	0.000064	0.006906	0.090642	0.328503	0.053164	0.347363	0.000000	0.000000	0.000000	0.000000	0.000000
8	0.000000	0.000067	0.000036	0.000092	0.000462	0.013029	0.123330	0.319594	0.030826	0.000000	0.000000	0.000000	0.000000	0.000000
9	0.000000	0.000004	0.000131	0.000078	0.000013	0.000912	0.021120	0.156731	0.325571	0.000000	0.000000	0.000000	0.000000	0.000000
						$(3)1/2$–$X^2\Sigma+1/2$								
$v'=0$	0.000002	0.000057	0.000400	0.002491	0.013257	0.048381	0.121107	0.211164	0.245963	0.199742	0.113853	0.038451	0.004524	0.000051
1	0.000028	0.000755	0.003923	0.016478	0.054711	0.112499	0.129055	0.063035	0.000478	0.054393	0.175248	0.218391	0.134081	0.034243
2	0.000216	0.004536	0.018057	0.052861	0.110648	0.119527	0.040456	0.002385	0.059184	0.058927	0.001918	0.058467	0.195200	0.194876
3	0.000894	0.014294	0.042688	0.083192	0.097065	0.033697	0.003920	0.060262	0.039865	0.000817	0.051054	0.039294	0.004767	0.141545
						$(1)3/2$–$X^2\Sigma+1/2$								
$v'=0$	0.976493	0.015687	0.002866	0.004000	0.000220	0.000398	0.000236	0.000000	0.000000	0.000000	0.000000	0.000000	0.000000	0.000000
1	0.019271	0.817655	0.159869	0.001927	0.000285	0.000521	0.000003	0.000000	0.000000	0.000000	0.000000	0.000000	0.000000	0.000000
2	0.000670	0.143170	0.626105	0.218721	0.010544	0.000051	0.000242	0.000000	0.000000	0.000000	0.000000	0.000000	0.000000	0.000000
3	0.001956	0.018533	0.186798	0.533009	0.231392	0.026954	0.000759	0.000000	0.000000	0.000000	0.000000	0.000000	0.000000	0.000000
4	0.001084	0.003901	0.022089	0.211342	0.441336	0.268946	0.044782	0.000000	0.000000	0.000000	0.000000	0.000000	0.000000	0.000000
5	0.000270	0.000208	0.001708	0.026577	0.267422	0.311047	0.312711	0.000000	0.000000	0.000000	0.000000	0.000000	0.000000	0.000000
6	0.000134	0.000497	0.000000	0.002093	0.044216	0.324610	0.216985	0.000000	0.000000	0.000000	0.000000	0.000000	0.000000	0.000000
7	0.000094	0.000048	0.000223	0.000000	0.003734	0.060400	0.352118	0.000000	0.000000	0.000000	0.000000	0.000000	0.000000	0.000000
						$(2)3/2$–$X^2\Sigma+1/2$								
$v'=0$	0.000005	0.000160	0.001014	0.005583	0.025973	0.082035	0.174625	0.263266	0.237744	0.147940	0.059396	0.011574	0.000231	0.000302
1	0.000072	0.001726	0.007985	0.028959	0.080861	0.133268	0.106890	0.018946	0.019348	0.137924	0.221833	0.171733	0.062878	0.006850
2	0.000444	0.008122	0.028147	0.068699	0.114064	0.085695	0.008341	0.025544	0.075168	0.024261	0.015123	0.153574	0.234070	0.133151
3	0.001887	0.025614	0.064048	0.096749	0.076464	0.007949	0.023664	0.062244	0.010184	0.021472	0.063865	0.008254	0.056128	0.222781
4	0.005823	0.057375	0.098715	0.079207	0.013459	0.015420	0.056215	0.010480	0.018687	0.044825	0.001751	0.034706	0.037119	0.007727
5	0.013104	0.091074	0.099009	0.027450	0.005603	0.051927	0.016773	0.012448	0.040966	0.001448	0.029084	0.025245	0.005140	0.046621
6	0.023467	0.109148	0.062336	0.000039	0.043234	0.033313	0.003366	0.042212	0.004752	0.023015	0.025112	0.003028	0.035918	0.001534
7	0.036552	0.106016	0.020316	0.019085	0.055807	0.001734	0.035028	0.017051	0.012699	0.031310	0.000297	0.031661	0.003976	0.022959
8	0.052050	0.085867	0.000431	0.051861	0.028088	0.011562	0.037256	0.000833	0.036176	0.001957	0.025776	0.010685	0.013989	0.019481
9	0.069548	0.057189	0.008529	0.060907	0.001791	0.038489	0.008713	0.024666	0.015229	0.013407	0.022855	0.004137	0.025565	0.000617

internuclear distances of the upper and lower states. The FC factors are in good accordance with the experimental value 0.96814 in $A^2\Pi$–$X^2\Sigma^+$ transition,[39] while differ from the values (0.930 and 0.928, respectively) in the recent theoretical literature.[10] For diagonal 1–1 and 2–2 vibrational transitions, similar to those calculated in the previous work (0.792 and 0.798, respectively),[10] the FC factors are computed to be 0.789 and 0.818, respectively. The 0–0 bands of the transitions $(3)1/2$–$X^2\Sigma+1/2$ and $(1)3/2$–$X^2\Sigma+1/2$ have very small FC factors because of the significantly different equilibrium internuclear distances between the upper and the lower electronic states.

The radiative lifetimes of the selected vibrational level v' have been calculated by the following formula:[42,43]

$$\begin{aligned}\tau_{v'} &= (A_{v'})^{-1} \\ &= \frac{3h}{64\pi^4 \left|a_0 \cdot e \cdot \overline{TDM}\right|^2 \Sigma_{v''} q_{v',v''} (\Delta E_{v',v''})^3} \\ &= \frac{4.936 \times 10^5}{(\overline{TDM})^2 \Sigma_{v''} q_{v',v''} (\Delta E_{v',v''})^3},\end{aligned}$$

where v' and v'' correspond to the upper and lower vibrational states, the energy difference $\Delta E_{v',v''}$ is in unit cm^{-1}, the averaged electronic transition dipole moment TDM is in atomic units, $q_{v',v''}$ is the FC factor, and the radiative lifetime $\tau_{v'}$ is in second.

Aside from the larger diagonal FC factors, the shorter spontontaneous radiative lifetime τ (10^{-9} s $\sim 10^{-6}$ s) can be applied for rapid laser cooling, which can provide a signifcant rate of rapid cycling. The radiative lifetimes $\tau_{v'}$ of $v' = 0$–3 for the lowest transitions are determined and listed in Table 5. It can be seen that our calculated radiative lifetimes $\tau_{v'}$ are all on the order of 10 ns, which are a bit smaller than the previous theoretical results.[10]

Table 5. The radiative lifetimes of the transitions $(2)1/2$–$X^2\Sigma+1/2$, $(3)1/2$–$X^2\Sigma+1/2$, $(1)3/2$–$X^2\Sigma+1/2$, and $(2)3/2$–$X^2\Sigma+1/2$.

Transition	Radiative lifetimes/ns			
	$v'=0$	$v'=1$	$v'=2$	$v'=3$
$(2)1/2$–$X^2\Sigma+1/2$	9.39	9.42	9.35	9.26
Calc.[a]	10.05	10.09	10.14	10.19
$(1)3/2$–$X^2\Sigma+1/2$	9.68	9.76	9.62	9.56
Calc.[a]	10.08	10.12	10.16	1020
$(3)1/2$–$X^2\Sigma+1/2$	11.55	11.07	10.55	10.32
$(2)3/2$–$X^2\Sigma+1/2$	12.84	12.35	11.93	12.05

[a]Ref. [10]

4. Conclusions

High-level *ab initio* calculations on the ground and low-lying excited states of MgCl have been carried out by employing the MRCI + Q method with relativistic corrections. The PECs of 14 Λ–S states are calculated and plotted with the aid of the avoided crossing rule. From the PECs of the bound states, the corresponding spectroscopic constants are obtained, and the constants of the $X^2\Sigma^+$ and $A^2\Pi$ states are in good agreement with previous measurements. The $B^2\Sigma^+$ state is characterized by the shallow potential well with large equilibrium internuclear distance, which is associated with the ion-pair dissociation limit $Mg^+(^2S_g) + Cl^-(^1S_g)$. The calculated PDMs exhibit two asymptotic limits because of the different dissociation product channels of Mg + Cl and $Mg^+ + Cl^-$ at large distance. The abrupt changes of PDMs and SO reveal the sharp changes of the electron configurations in the wavefunctions of the $A^2\Pi$ and $C^2\Pi$ states at their avoided crossing point. The SOC effect splits 14 Λ–S states into 30 Ω states. The spectroscopic results indicate that the SOC effect brings little effect on the ground state $X^2\Sigma^+$, except for the dissociation energy. The computed spliting between the $\Omega = 1/2$ and $3/2$ components of the $A^2\Pi$ state is 53.61 cm^{-1}, which agrees well with the experimental observation 54.47 cm^{-1}. Under the influence of the SOC effect, many avoided crossings of the PECs are generated. The strong coupling between the $A^2\Pi$ and $C^2\Pi$ states at their crossing region are analyzed with the help of the Λ–S compositions for the Ω states. The TDMs, FC factors, and radiative lifetimes are determined. The radiative lifetimes for the four transitions are all evaluated on the order of 10 ns. The present computational work should shed light on the spectroscopy of low-lying electronic state and pave further experimental studies on the laser cooling of MgCl molecule.

Acknowledgment

The authors gratefully acknowledge the High Performance Computing Center (HPCC) of Jilin University for supercomputer time.

References

[1] Barber B E, Zhang K Q, Guo B and Bernath P F 1995 *J. Mol. Spectrosc.* **169** 583
[2] Buckingham A D and Olegagio R M 1993 *Chem. Phys. Lett.* **212** 253
[3] Baucchlicher C W, Langhoff S R, Steimle T C and Shirley J E 1990 *J. Chem. Phys.* **93** 4179
[4] Walters O H and Barratt S 1928 *Proc. R. Soc. London Ser. A* **118** 120
[5] Morgan F 1936 *Phys. Rev.* **50** 603
[6] Sadygov R G, Rostas J, Taieb G and Yarkony D 1997 *J. Chem. Phys.* **106** 4091
[7] Törring T, Ernst W E and Kindt S 1989 *J. Chem. Phys.* **90** 4927
[8] Törring T, Ernst W E and Kändler J 1984 *J. Chem. Phys.* **81** 4614
[9] Rice S F, Martin H and Field R W 1985 *J. Chem. Phys.* **82** 5023
[10] Wan M J, Shao J X, Gao Y F, Huang D H, Yang J S, Cao Q L, Jin C G and Wang F H 2015 *J. Chem. Phys.* **143** 024302
[11] Wan M J, Huang D H, Shao J X, Yu Y, Li S and Li Y Y 2015 *J. Chem. Phys.* **143** 164312
[12] Singh M, Ghodgaokar G S and Saksena M D 1987 *Can. J. Phys.* **65** 1594
[13] Hirao T, Bernath P F, Fellows C E, Gutterres R F and Vervloet M 2002 *J. Mol. Spectrosc.* **212** 53
[14] Ohshima Y and Endo Y 1993 *Chem. Phys. Lett.* **213** 95
[15] Rao V S N and Rao P T 1963 *Indian J. Phys.* **37** 640
[16] Darji A B, Shah N R, Shah P M, Sureshkumar M B and Desai G S 1985 *Pramana* **25** 571

[17] Singh M, Saksena M D and Ghodgaokar G S 1988 *Can. J. Phys.* **66** 570

[18] Parl, G, Rostas J, Taieb G and Yarkony D R 1990 *J. Chem. Phys.* **93** 6403

[19] Bogey M, Demuynck C and Destombes J L 1989 *Chem. Phys. Lett.* **155** 265

[20] Wu D L, Tan B, Qin J Y, Wan H J, Xie A D, Yan B and Ding D J 2015 *Spectrochim. Acta Part. A* **150** 499

[21] Werner H J, Knowles P J, Lindh R, Manby F R, Schütz M, Celani P, Korona T, Mitrushenkov A, Rauhut G, Adler T B, Amos R D, Bernhardsson A, Berning A, Cooper D L, O Deegan M J, Dobbyn A J, Eckert F, Goll E, Hampel C, Hetzer G, Hrenar T, Knizia G, Köppl C, Liu Y, LloydA W, Mata R A, May A J, McNicholas S J, Meyer W, Mura M E, Nicklass A, Palmieri P, Pflüger K, Pitzer R, Reiher M, Schumann U, Stoll H, Stone A J, Tarroni R, Thorsteinsson T, Wang M and Wolf A 2012 *MOLPRO*, Version 2012.1, a package of *ab initio* programs

[22] Werner H J , Knowles P J, Knizia G, Manby F R and Schütz M 2012 *WIREs Comput. Mol. Sci.* **2** 242

[23] Werner H J and Knowles P J 1985 *J. Chem. Phys.* **82** 5053

[24] Knowles P J and Werner H J 1985 *Chem. Phys. Lett.* **115** 259

[25] Werner H J and Knowles P J 1988 *J. Chem. Phys.* **89** 5803

[26] Knowles P J and Werner H J 1988 *Chem. Phys. Lett.* **145** 514

[27] Li R, Wei C L, Sun Q X, Sun E P, Xu H F and Yan B 2013 *J. Phys. Chem. A* **117** 2373

[28] Li R, Zhang X M, Jin M X, Yan B and Xu H F 2014 *Chem. Phys. Lett.* **594** 6

[29] Langhoff S R and Davidson E R 1974 *Int. J. Quantum Chem.* **8** 61

[30] Woon D E and Dunning T H 1993 *J. Chem. Phys.* **98** 1358

[31] Wilson A K, Woon D E, Peterson K A and Dunning T H 1999 *J. Chem. Phys.* **110** 7667

[32] Berning A, Schweizer M, Werner H J , Knowles P J and Palmieri P 2000 *Mol. Phys.* **98** 1823

[33] Le Roy R J 2007 *LEVEL* 8.0: A *Computer Program for Solving the Radial Schrdinger Equation for Bound and Quasibound Levels*, University of Waterloo Chemical Physics Research Report CP-663, University of Waterloo, Ontario

[34] Wu D L, Tan B, Wen Y F, Zeng X F, Xie A D and Yan B 2016 *Spectrochim. Acta Part. A* **161** 101

[35] Drakes J A 1995 *J. Quantum Spectrosc. Radiat. Transfer* **54** 1039

[36] Rostas J, Shafizadeh N, Taieb G, Bourguignon B and Prisant M G 1990 *Chem. Phys.* **142** 97

[37] Kang S Y, Gao Y F, Kuang F G, Gao T, Du J G and Jiang G 2015 *Phys. Rev. A* **91** 042511

[38] Zhao S T, Yan B, Li R, Wu S and Wang Q L 2017 *Chin. Phys. B* **26** 023105

[39] Wan M J, Jin C G, Yu Y, Huang D H and Shao J X 2017 *Chin. Phys. B* **26** 033101

[40] Wei C L, Zhang X M, Ding D J and Yan B 2016 *Chin. Phys. B* **25** 013102

[41] Moore C E 1971 *Atomic Energy Levels*, National Bureau of Standards, Washington, DC

[42] Okabe H 1978 *Photochemistry of Small Molecules* (New York: Wiley-Interscience)

[43] Zou W L and Liu W J 2005 *J. Comput. Chem.* **26** 106